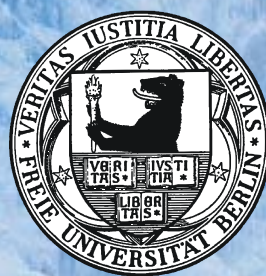


Freezing Hot Electrons

Electron Transfer and Solvation Dynamics
at D₂O and NH₃ – Metal Interfaces

Im Fachbereich Physik der
Freien Universität Berlin
eingereichte Dissertation



Anne Julia Stähler

May 2007

An electronic version of this work (PDF) will be available on the dissertation server of the Freie Universität Berlin (<http://www.diss.fu-berlin.de>).

This work was done between July 2004 and May 2007 in the group of Professor Martin Wolf at the Physics Department of the Freie Universität Berlin.

Berlin, in May 2007

1st referee: Prof. Dr. Martin Wolf

2nd referee: Prof. Dr. Nikolaus Schwentner

Date of defense: July 5, 2007

Wer spricht von siegen? Überstehn ist alles.

Rainer Maria Rilke

Abstract

Heterogeneous electron transfer is highly important for a variety of different fields, such as photochemistry, development of nanoscale molecular electronic devices, and solar cells. Understanding the fundamental processes of charge transfer is thus of vital significance for future applications. As excess electrons in polar environments, such as water or ammonia, dynamically localize and stabilize (solvate) by rearrangement of surrounding polar molecules, they are a model system for electron transfer (ET) phenomena if investigated in the vicinity of a metal surface: The transient degree of confinement of the solvated electrons subsequently changes the electronic coupling degree to unoccupied substrate states.

The present work investigates the electron transfer and solvation dynamics at the D₂O/Cu(111), D₂O/Ru(001), and NH₃/Cu(111) interfaces using femtosecond time-resolved two-photon photoelectron spectroscopy. Within this framework, the influence of the substrate, adsorbate structure and morphology, solvation site, coverage, temperature, and solvent on the electron dynamics are studied, yielding microscopic insight into the underlying fundamental processes. Transitions between different regimes of ET, substrate-dominated, barrier-determined, strong, and weak coupling are observed by systematic variation of the interfacial properties and development of empirical model descriptions. It is shown that the fundamental steps of the interfacial electron dynamics are similar for all investigated systems: Metal electrons are photoexcited to unoccupied metal states and transferred into the adlayer via the adsorbate's conduction band. The electrons localize at favorable sites and are stabilized by reorientations of the surrounding polar solvent molecules. Concurrently, they decay back to the metal substrate, as it offers a continuum of unoccupied states.

However, the detailed characteristics vary for the different investigated interfaces: For amorphous ice-metal interfaces, the electron transfer is initially, right after photoinjection, dominated by the substrate's electronic surface band structure. With increasing solvation, a transient barrier evolves at the interface that increasingly screens the electrons from the substrate. Tunneling through this barrier becomes the rate-limiting step for ET. The competition of electron decay and solvation leads to lifetimes of the solvated electrons in the order of 100 fs. Furthermore, it is shown that the electrons bind in the bulk of the ice *layers*, but on the edges of adsorbed D₂O *clusters* and that the ice morphology strongly influences the electron dynamics. For the amorphous NH₃/Cu(111) interface, two isomers of solvated electrons are found. One exhibits electron dynamics on femtosecond, the other one on picosecond timescales. A similar transition between ET regimes is observed as for ice, but, furthermore, it is shown that – depending on layer thickness – the weak coupling limit is reached, where ET is mediated by thermally activated rearrangement of the solvent. Upon crystallization, the electron dynamics change significantly. Instead of femto- or picoseconds, the electrons reside for minutes in the adlayer. The observation of their formation dynamics allows analysis of their energetic stabilization over 17 orders of magnitude in time. It is shown that their high degree of screening is achieved by localization at orientational defects at the adsorbate-vacuum interface.

Deutsche Kurzzusammenfassung

Heterogener Elektronentransfer spielt eine entscheidende Rolle in einer Vielzahl technologisch relevanter Bereiche wie beispielsweise der Photovoltaik oder Molekularelektronik, so dass ein tiefgehendes Verständnis der zugrundeliegenden Prozesse von großer Bedeutung ist. Die Solvatisierung von Überschusselektronen in polaren Lösungsmitteln, d.h. ihre Lokalisierung und Stabilisierung, reduziert zeitabhängig ihre räumliche Ausdehnung. Findet dies nahe einer Metallgrenzfläche statt, ändert sich demzufolge fortlaufend der Wellenfunktionsüberlapp mit dem Substrat. Da sich so die elektronische Ankopplung der Überschussladung sukzessiv verringert, stellen solvatisierte Elektronen ein Modellsystem für Ladungstransferprozesse dar.

In der vorliegenden Arbeit wird die Elektronentransfer- (ET) und Solvatisierungsdynamik an den D₂O/Cu(111), D₂O/Ru(001) und NH₃/Cu(111) Grenzflächen mit Hilfe zeitaufgelöster Zwei-Photonen Photoemissionsspektroskopie untersucht. Die Erforschung des Einflusses von Substrat, Adsorbatstruktur, Solvatisierungsart, Bedeckung, Temperatur und Lösungsmittel auf die Elektronendynamik ermöglicht Einsicht in die beteiligten Prozesse. Mit Hilfe dieser systematischen Veränderung der Molekül-Metall Grenzflächen und durch die Neuentwicklung von empirischen Modellen zur Beschreibung der Elektronendynamik, wird der Übergang zwischen substrat- und barrierenbestimmtem ET sowie zwischen den Grenzfällen starker und schwacher Kopplung beobachtet. Die grundlegenden Prozesse der Grenzflächendynamik sind hierbei für alle untersuchten Systeme vergleichbar: Angeregt durch einen ultrakurzen Laserpuls werden Metallelektronen über das Leitungsband in die Adsorbatschicht transferiert. Dort lokalisieren sie in Potentialminima und werden durch Umorientierung der polaren Moleküle energetisch stabilisiert. In Konkurrenz dazu zerfällt die Population gleichzeitig aufgrund des Kontinuums an unbesetzten elektronischen Zuständen in das Substrat zurück.

Trotz dieser Gemeinsamkeiten unterscheidet sich die Elektronendynamik an den verschiedenen Grenzflächen: Im Fall von amorphen Eisschichten ist der ET direkt nach der Anregung alleine durch die Oberflächenbandstruktur des Metalls bestimmt. Im Laufe der Solvatisierung entwickelt sich allerdings eine Tunnelbarriere zwischen Elektron und Substrat, die im Folgenden die Transferrate in der Größenordnung von 100 fs bestimmt. Des Weiteren wird gezeigt, dass die Solvatisierung im Volumen der Eisschichten und an der Oberfläche adsorbierter Eiscluster stattfindet, deren Morphologie die Elektronendynamik stark beeinflusst. An der NH₃/Cu(111) Grenzfläche findet Solvatisierung in zwei verschiedenen Isomeren statt, von denen das eine fs- und das andere ps-Dynamik aufweist. Ein zu Eis vergleichbarer Übergang zwischen substrat- und barrierenbestimmtem ET findet statt, jedoch ermöglicht die hohe Lebensdauer im Ammoniak – je nach Bedeckung – die Beobachtung des Überganges zum Grenzfall schwacher Kopplung, wo der ET durch thermisch aktivierte Umordnung des Lösungsmittels vermittelt wird. Die Kristallisierung der Adsorbatschichten verändert die Elektronendynamik drastisch, denn selbst nach mehreren Minuten können noch Überschusselektronen nachgewiesen werden. Durch die Beobachtung ihrer Bildung kann schließlich die Stabilisierungsdynamik über 17 Größenordnungen der Zeit verfolgt werden. Der hierfür nötige hohe Grad an Abschirmung wird durch Lokalisierung an Defekten an der Vakkumgrenzfläche erreicht.

Abbreviations

2PPE	Two-Photon Photoelectron
ASW	Amorphous Solid Water
BBO	β -Barium Borate
BL	Bilayer
BLYP	Becke-Lee-Yang-Parr
CB	Conduction Band
CCD	Charge-Coupled Device
CFC	Chlorofluorocarbon
CSS	Conformational Substates
CTTS	Charge Transfer to Solvent
cw	Continuous Wave
DAQ	Data Acquisition Time
DFG	Difference Frequency Generation
DFT	Density Functional Theory
DNA	Deoxyribonucleic Acid
DOS	Density of States
e ⁻	Electron
e _{CB}	(Spectral Feature of) Conduction Band Electrons
e _S	(Spectral Feature of) Solvated Electrons
e _T	(Spectral Feature of) Trapped Electrons
ET	Electron Transfer
fcc	Face-Centered Cubic
H-bond	Hydrogen Bond
hcp	Hexagonal Closed Packed
HET	Heterogeneous Electron Transfer
HOMO	Highest Occupied Molecular Orbital
HT	High-Temperature
IPS	Image Potential State
IR	Infrared
KDP	Potassium Dihydrogen Phosphate
LEED	Low Energy Electron Diffraction
LUMO	Lowest Unoccupied Molecular Orbital
MCP	Micro Channel Plate
ML	Monolayer
OPA	Optical Parametric Amplifier

QMS	Quadrupole Mass Spectrometer
RegA	Regenerative Amplifier
SAC	Solvent Anion Complex
SB	Switch Box
SFG	Sum Frequency Generation
SHG	Second Harmonic Generation
STM	Scanning Tunneling Microscopy
TD	Thermal Desorption
TDS	Thermal Desorption Spectroscopy
TOF	Time of Flight
UHV	Ultrahigh Vacuum
UV	Ultraviolet
VB	Valence Band
VBE	Vertical Binding Energy
VIS	Visible
XC	Cross-Correlation

Table of Contents

Abstract	7
Deutsche Kurzzusammenfassung	9
Abbreviations	10
Table of Figures	14
Table of Tables	17
1. Introduction	19
2. Investigated Processes and Interfaces	24
2.1 Electron Transfer	24
2.1.1 Tunneling and Wave Function Overlap	25
2.1.2 Marcus Theory	28
2.1.3 Truhlar Concept	31
2.2 Electron Solvation	34
2.3 Transfer and Solvation at Interfaces	38
2.3.1 Ultrafast Dynamics in Amorphous Ice on Cu(111)	39
2.3.2 Ultraslow Dynamics in Crystalline Ice on Cu(111)	41
<i>Summary</i>	43
2.4 Ice- and Ammonia-Metal Interfaces	44
2.4.1 Water-Ice and Ammonia	44
2.4.2 Electronic Properties of Cu(111) and Ru(001)	51
2.4.3 D ₂ O and NH ₃ on Metal Surfaces	55
3. Experimental Details	59
3.1 Time-Resolved Two-Photon Photoelectron Spectroscopy	59
3.2 Experimental Setup	62
3.2.1 UHV Components	62
3.2.2 Laser System	65
3.2.3 Time of Flight Detection and Signal Processing	69
3.3 Sample Preparation and Characterization	73
3.3.1 Metal Substrates	73
3.3.2 Adsorbate Layers	74
3.4 Data Analysis	78
3.4.1 Photoelectron Spectra	79
3.4.2 Population Dynamics	82
<i>Outline</i>	86

4. Electron Transfer and Solvation at Ice – Metal Interfaces	87
4.1 Ultrafast Electron Dynamics at Amorphous Ice-Metal Interfaces	87
4.1.1 Cross-Over between Substrate- and Barrier-Determined ET	88
4.1.2 Impact of the Ice Structure	96
4.1.3 Surface vs. Bulk Solvation	104
4.1.4 Discussion: Tunneling vs. Marcus	110
<i>Conclusions</i>	116
4.2 Freezing Hot Electrons in Crystalline Ice	118
4.2.1 Electron Solvation from Femtoseconds to Minutes	118
4.2.2 Thermally Activated Electron Solvation via Conformational Substates	126
<i>Conclusions</i>	132
5. Electron Transfer and Solvation Dynamics at the NH₃/Cu(111) Interface	133
5.1 Ultrafast Electron Dynamics in Amorphous Ammonia Adlayers	133
5.1.1 Formation Dynamics of Solvated Electrons	133
5.1.2 Charge Transfer mediated by Tunneling	139
5.1.3 Tuning the Coupling Degree	146
5.1.4 Discussion: Water vs. Ammonia	149
<i>Conclusions</i>	152
5.2 Ultrafast and Ultraslow Dynamics in Crystalline Ammonia	154
5.2.1 Transition to the Well-Ordered Phase: IPS	154
5.2.2 Freezing Hot Electrons in Crystalline Ammonia	157
5.2.3 Discussion: Electron Trapping in Crystalline Solvents	159
<i>Conclusions</i>	162
6. Summary and Conclusions	164
Appendix	169
A. Dispersion Measurements of Amorphous NH₃/Cu(111)	169
B. The First Bilayer of D₂O/Ru(001)	172
C. Temperature Calibration	175
Bibliography	177
Publications	190
Acknowledgements	191

Table of Figures

Chapter 1

Fig. 1.01 2PPE Experiment of Electron Transfer and Solvation Phenomena

21

Chapter 2

Fig. 2.01	Two Limits of Electron Transfer at Interfaces	25
Fig. 2.02	Scattering Processes in Metals	26
Fig. 2.03	Relaxation Processes of an Interfacial Electron	27
Fig. 2.04	Marcus Picture for Homogeneous Charge Transfer	28
Fig. 2.05	Marcus Picture for Heterogeneous Charge Transfer	30
Fig. 2.06	2D Model for Homogeneous Proton Transfer	31
Fig. 2.07	Optical Absorption Spectra of Liquid Water and Ammonia	35
Fig. 2.08	Photoelectron Spectra of $(D_2O)_{50}^-$ Clusters under Varying Baking Pressures	36
Fig. 2.09	Time-Resolved 2PPE Spectra of Amorphous $D_2O/Cu(111)$	39
Fig. 2.10	Fundamental Steps of Electron Transfer and Solvation	40
Fig. 2.11	Ultralong-Living Electrons in Crystalline $D_2O/Ru(001)$	42
Fig. 2.12	Process of Electron Trapping	42
Fig. 2.13	H-bond and A-H-Group Potential	44
Fig. 2.14	The Water Molecule and its Orbitals	45
Fig. 2.15	Simplified Phase Diagram of Water	46
Fig. 2.16	Structure of Ice I_h and Point Defects	47
Fig. 2.17	Comparison of a Crystalline and an Amorphous Solid	49
Fig. 2.18	Ammonia	50
Fig. 2.19	Projected Surface Band Structure of $Cu(111)$	51
Fig. 2.20	Image Potential State	52
Fig. 2.21	Electronic Surface Bandstructures and Densities of States of the Investigated Substrates	54
Fig. 2.22	The Water Bilayer on $Ru(001)$	56
Fig. 2.23	STM Image of an H_2O Multilayer on $Cu(111)$	57
Fig. 2.24	Monolayer Adsorption of NH_3 on $Cu(111)$	57

Chapter 3

Fig. 3.01	2PPE Spectroscopy	59
Fig. 3.02	Excitation Mechanisms	60
Fig. 3.03	UHV Components	62
Fig. 3.04	Sample Holder	63
Fig. 3.05	Gas System	64
Fig. 3.06	Laser System	66

Fig. 3.07	Pulse Characterization of the Compressed RegA Output	67
Fig. 3.08	Experimental Setup	69
Fig. 3.09	Signal Processing	70
Fig. 3.10	Potential Diagram of Spectrometer and Sample	71
Fig. 3.11	Background Pressure During NH ₃ Dosage	74
Fig. 3.12	TD Spectra of D ₂ O/Ru(001)	75
Fig. 3.13	TD Spectra of NH ₃ /Cu(111)	77
Fig. 3.14	Time-Resolved 2PPE Measurement of the Bare Ru(001) Surface	78
Fig. 3.15	Final State Energy Axis Determination	80
Fig. 3.16	Energy Axes	81
Fig. 3.17	Single Exponential Fit	85
Chapter 4		
Fig. 4.01	Time-Resolved 2PPE Spectra of Amorphous D ₂ O on Metal Surfaces	88
Fig. 4.02	Energetic Shift of e _S for D ₂ O/Cu(111) and Ru(001)	89
Fig. 4.03	Population Decay of e _S for D ₂ O/Cu(111) and Ru(001)	90
Fig. 4.04	Substrate-Dominated and Barrier-Determined Electron Transfer	92
Fig. 4.05	Real and Effective Barriers	94
Fig. 4.06	Best Fit of Empirical Model	95
Fig. 4.07	STM Scheme	97
Fig. 4.08	Apparent Height	97
Fig. 4.09	STM Images of Porous and Compact Amorphous Ice Clusters on Cu(111)	98
Fig. 4.10	2PPE Data of Porous and Compact Amorphous Ice Clusters	99
Fig. 4.11	Stable and Metastable Structures of D ₂ O/Cu(111)	100
Fig. 4.12	Data Analysis for Porous, Compact, Facetted, and Pyramidal Clusters	101
Fig. 4.13	Empirical Model for Porous and Compact Clusters	103
Fig. 4.14	Xe Overlayer Experiment	105
Fig. 4.15	Influence of the Xe Adlayer	106
Fig. 4.16	Xe Adsorption on top of the Ice Multilayer	106
Fig. 4.17	Binding Sites of Solvated Electrons at the D ₂ O/Cu(111) Interface	107
Fig. 4.18	2D Model for Heterogeneous Charge Transfer	111
Fig. 4.19	Influence of Temperature on HET from an Equilibrated Donor	112
Fig. 4.20	Thermally Activated Electron Transfer	113
Fig. 4.21	Strong and Weak Coupling	114
Fig. 4.22	Temperature Dependence of ET for D ₂ O/Cu(111) and Ru(001)	115
Fig. 4.23	2PPE Spectra of Crystalline D ₂ O/Ru(001)	119
Fig. 4.24	Pump-Probe Schemes for Ultrafast and Ultraslow Dynamics	121
Fig. 4.25	Illustration of Signal-to-Background Ratio	122
Fig. 4.26	Electron Dynamics in Crystalline D ₂ O on Femtosecond Timescales	123
Fig. 4.27	Population Dynamics of Ultralong-Living Electrons	124
Fig. 4.28	Dynamics Ranging Over 17 Orders of Magnitude in Time	126
Fig. 4.29	Conformational Substates	127
Fig. 4.30	Temperature Dependence of the Trapped Electrons	128
Fig. 4.31	DFT Calculation of Orientational Defect Sites for Electron Trapping	130

Table of Figures

Chapter 5

Fig. 5.01	Time-Resolved 2PPE Data of 8.5 ML Amorphous NH ₃ /Cu(111)	134
Fig. 5.02	Shift of Peak Maximum of 8.5 ML Amorphous NH ₃ /Cu(111)	135
Fig. 5.03	Population Dynamics of 8.5 ML Amorphous NH ₃ /Cu(111)	136
Fig. 5.04	Fundamental Steps of Electron Solvation in Amorphous NH ₃ /Cu(111)	139
Fig. 5.05	Coverage Dependence of Work Function and Peak Shift	140
Fig. 5.06	Coverage Dependence of Population Decay	141
Fig. 5.07	Early Time Dynamics	142
Fig. 5.08	Charge Transfer Mediated by Tunneling	143
Fig. 5.09	Xenon Overlayer Experiment	144
Fig. 5.10	Elastic Electron Scattering	145
Fig. 5.11	Temperature Dependence of Electron Population Dynamics for 12 ML NH ₃ /Cu(111)	146
Fig. 5.12	Temperature Dependence of Characteristic Times and Rates	147
Fig. 5.13	Temperature Dependence of Population Dynamics for 8 ML NH ₃ /Cu(111)	148
Fig. 5.14	Electron Solvation in Ice and Ammonia Layers	150
Fig. 5.15	Electron Population Decay at Ice- and Ammonia-Metal Interfaces	151
Fig. 5.16	ET at the NH ₃ /Cu(111) Interface	152
Fig. 5.17	Temperature 2PPE and TD Spectroscopy	154
Fig. 5.18	Work Function and IPS of NH ₃ /Cu(111)	155
Fig. 5.19	Population Dynamics of the IPS	156
Fig. 5.20	Pump-Probe Experiment on Macroscopic Timescales	157
Fig. 5.21	Time-Resolved 2PPE Spectra of Crystalline NH ₃ /Cu(111)	158
Fig. 5.22	Time-Dependent Peak Shift of e _T	158
Fig. 5.23	Temperature-Dependent Peak Shift of Trapped Electrons	159
Fig. 5.24	Comparison of the e _T Dynamics for NH ₃ and D ₂ O	160
Fig. 5.25	Harmonic Potentials of NH ₃ and D ₂ O	162

Appendix

Fig. A.01	Experimental Setup for Angular-Resolved 2PPE	169
Fig. A.02	Impact of Finite k-Space Width on 2PPE Intensity	170
Fig. A.03	Dispersion of Solvated Electrons in Amorphous Ammonia	171
Fig. B.01	TD Spectra 1 BL D ₂ O/Ru(001) Before and After Electron Irradiation	172
Fig. B.02	Work Function Change as a Function of Electron Irradiation	173
Fig. C.01	TD Spectra of Rare Gases Adsorbed on Cu(111)	175
Fig. C.02	Temperature Calibration	176

Table of Tables

Chapter 2

Tab. 2.01	Image Potential States on the Bare Ru(001) Surface	54
Tab. 2.02	Work Function Change for Different Bilayer Structures	56

Chapter 4

Tab. 4.01	Fit Parameters for the D ₂ O Multilayer, Porous, and Compact Clusters	103
Tab. 4.02	Parameters of CSS Model	129

Chapter 5

Tab. 5.01	Fit Parameters for the Population Decay of 8.5 ML Amorphous NH ₃ /Cu(111)	137
Tab. 5.02	Parameters of CSS Model	161

